

A Compressible Turbulence Model for Pressure—Strain

Hechmi Khlifi * and Adnen Bourehla

Laboratory of Aeronautical Structure and Control of System Flows, SACES (UR17DN01),
School of Military Aviation, Borj El Amri 1142, Tunisia; bourehla@gmail.com

* Correspondence: khlifihachmi@yahoo.fr; Tel.: +216-2-5371690

Abstract: This work focuses on the performance and validation of compressible turbulence models for the pressure-strain correlation. Considering the Launder Reece and Rodi (LRR) incompressible model for the pressure-strain correlation, Adumitroaie et al., Huang et al., and Marzougui et al., used different modeling approaches to develop turbulence models, taking into account compressibility effects for this term. Two numerical coefficients are dependent on the turbulent Mach number, and all of the remaining coefficients conserve the same values as in the original LRR model. The models do not correctly predict the compressible turbulence at a high-speed shear flow. So, the revision of these models is the major aim of this study. In the present work, the compressible model for the pressure-strain correlation developed by Khlifi–Lili, involving the turbulent Mach number, the gradient, and the convective Mach numbers, is used to modify the linear mean shear strain and the slow terms of the previous models. The models are tested in two compressible turbulent flows: homogeneous shear flow and the newly developed plane mixing layers. The predicted results of the proposed modifications of the Adumitroaie et al., Huang et al., and Marzougui et al., models and of its universal versions are compared with direct numerical simulation (DNS) and experiment data. The results show that the important parameters of compressibility in homogeneous shear flow and in the mixing layers are well predicted by the proposal models.

Keywords: turbulence; compressible; model; pressure-strain; shear flow; mixing layers



Citation: Khlifi, H.; Bourehla, A. A Compressible Turbulence Model for Pressure—Strain. *Fluids* **2022**, *7*, 34. <https://doi.org/10.3390/fluids7010034>

Academic Editor: Martin Skote

Received: 31 July 2021

Accepted: 21 August 2021

Published: 14 January 2022

Publisher's Note: MDPI stays neutral with regard to jurisdictional claims in published maps and institutional affiliations.



Copyright: © 2022 by the authors. Licensee MDPI, Basel, Switzerland. This article is an open access article distributed under the terms and conditions of the Creative Commons Attribution (CC BY) license (<https://creativecommons.org/licenses/by/4.0/>).

1. Introduction

Compressible turbulence modelling is an essential element for many industrial problems. A better understanding of the compressibility effects is highly relevant in the design of aerospace, supersonic, and hypersonic flights; combustion field; and other engineering problems. Firstly, attention is paid to study the compressibility effects on homogeneous shear flow (the mean velocity is $(Sx_2, 0, 0)$, $S = \text{cte}$), which is a useful problem because this flow summarizes some of the important compressibility properties in a simplified setting. In addition, this flow has excessively been used in calibration and evaluating turbulence models. In this context, the DNS results of Blaisdell et al. [1] and Sarkar et al. [2] show that there are significant turbulence changes when the compressibility increases as the turbulent kinetic energy growth rate decrease with the increasing turbulent Mach number, $M_t = \sqrt{2K/\bar{a}}$, $\bar{a} = \sqrt{\gamma R \bar{T}}$. Both studies show that the dilatational terms, π_d and ε_c , on the R.H.S of the turbulent kinetic energy equation were found to be much smaller compared with the control compressibility effects. Sarkar [3], Simone et al. [4], and Hamba [5] developed DNS results and reached a similar conclusion concerning the role of the dilatational terms. It has been found in their DNS results that the structural compressibility effects affect the pressure field and then the pressure-strain, which is recognized as the main factor responsible for the strong changes in the magnitude of the Reynolds stress anisotropies, and thereafter the reduced trend of the growth rate of the turbulent kinetic energy when the compressibility increases. Similar conclusions are confirmed by the DNS results of Vreman et al. [6]; the experimental data of Goebel et al. [7] and Samimy et al. [8]; and, more recently, the DNS data of Pantano et al. [9] and Foysi et al. [10], in which it

is reported that the compressibility effects on the pressure-strain are the main cause of the changes in the planar compressible mixing layers. Thus, we argue that the pressure-strain correlation is one of the mean terms contributing to the reduced growth rate and the changes of the Reynolds stress arising from the compressibility effects. Modeling the turbulent pressure-strain correlation occurs mainly at a high speed. Three independent compressible pressure-strain models, by Adumitroaie et al. [11], Huang et al. [12], and Marzougui et al. [13], are considered in this study. These models are derived by considering different variable density extensions of the Launder et al. LRR model [14], which account for the compressibility effects by using the turbulent Mach number. It has been shown that these models may be able to reproduce low and moderate compressibility effects. However, when the compressibility effects are more significant, the models do not correctly predict the decrease in the spreading rate of the mixing layers, as it is observed in [7–10], nor the reduction in the growth rate of turbulent kinetic energy [3–5]. The deficiencies of this closure are probably because LRR-compressibility correction models seem to be insufficient to induce important variation in calculations in accordance with the anisotropy turbulence strong changes when the compressibility is higher. Thus, one can see that in the models [11–13], the two coefficients that affect the linear term in relation to the Reynolds stress anisotropy and the mean strain are modified, which then become a function of the turbulent Mach number. All of the other remaining coefficients that affect the mean shear and the return to isotropy terms are conserved as in the LRR model [14], without any modification. However, modification of these models taking into account structural compressibility effects is needed for the pressure-strain correlation coefficient models. The present work focuses on this major issue. For this, more attention is paid to the results and the analysis of the DNS [3,4], in which some important compressibility discrepancies for homogeneous turbulent shear flows can be found. It has been argued that the gradient Mach number, $M_g = Sl/\bar{a}(S = \sqrt{\tilde{U}_i, j \tilde{U}_i, j})$, where S and l are the mean shear constant and integral length scale, respectively, is an appropriate parameter in addition to the turbulent Mach number for studying the structural compressibility effects and must be added to M_t in the compressible modelling concept. Similar recommendations have been suggested in different experimental [7,8] and DNS [9] data, which identify the convective Mach number, $M_c = (U_1 - U_2)/(a_1 + a_2)$, where U_1 , a_1 and U_2 , a_2 denoting the velocity and the speed sound in the high speed stream and in the low speed stream, respectively, as an appropriate parameter in order to study the compressibility effects on the planar mixing layer as in [7,8,15].

In the present study, a revision of the models by Adumitroaie et al. [11], Huang et al. [12], and Marzougui et al. [13] for pressure-strain is considered, making the model coefficients as a function of M_t , M_g , and M_c . The proposed models are tested in different compressible turbulent homogeneous shear flow and compressible mixing layers cases.

2. Basic Equations

In general, compressible turbulent flow is described by continuity, Navier–Stokes, energy, and state equations. It is well known that the basic equations of the mean quantities used in describing turbulence closure schemes are essentially those using the Favre average. These equations are formally similar to those governed by incompressible turbulent flows. Obviously, this technique gives reason to the extension of the incompressible turbulent models to study compressible turbulent flows. This is one of the essential advantages provided by the density weighting technique for modeling compressible turbulence. For this study, the Favre averaged continuity, momentum, and specific internal energy equations are respectively written as follows [11,16]:

$$\frac{\partial}{\partial t} \bar{\rho} + \frac{\partial}{\partial x_i} (\bar{\rho} \tilde{U}_i) = 0, \quad (1)$$

$$\frac{\partial}{\partial t} (\bar{\rho} \tilde{U}_i) + \frac{\partial}{\partial x_i} (\bar{\rho} \tilde{U}_i \tilde{U}_j) = \frac{\partial}{\partial x_j} (\tilde{\tau}_{ij} + \overline{\tau''_{ij}} - \frac{\partial}{\partial x_j} \overline{\rho u''_i u''_j} - \bar{p} \delta_{ij}), \quad (2)$$

$$\frac{\partial}{\partial t} \overline{\rho c_v \tilde{T}} + \frac{\partial}{\partial x_j} \overline{\rho c_v \tilde{T} \tilde{U}_j} = -\phi_e + \pi_d - \frac{\partial}{\partial x_j} (\overline{c_v \rho u''_j T''}) \tag{3}$$

where $\phi_e = \overline{p} \frac{\partial}{\partial x_i} (\tilde{U}_i + \overline{u''_i}) + \frac{\partial}{\partial x_i} (\overline{\kappa \frac{\partial}{\partial x_i} T}) + \overline{\tau_{ij} u_{i,j}}$, $\tilde{\tau}_{ij} = 2\overline{\mu} \tilde{S}_{ij} - \frac{2}{3} \overline{\mu} \tilde{U}_{k,k} \delta_{ij}$

3. Turbulence Models

The turbulence models used in this work are closely related to the standard Reynolds stress model from which the Favre averaged Reynolds stress, $\overline{\rho u''_i u''_j} / \overline{\rho}$, is described by the following equations [11,16]:

$$\frac{\partial}{\partial t} (\overline{\rho} R_{ij}) + \frac{\partial}{\partial x_m} (\overline{\rho} \tilde{U}_m R_{ij}) = Pr_{ij} + D_{ij} + P_{ij} + \varepsilon_{ij} + V_{ij} \tag{4}$$

where the symbols Pr_{ij} , D_{ij} , P_{ij} , ε_{ij} , and V_{ij} represent the turbulent production, turbulent diffusion, pressure-strain correlation, turbulent dissipation, and the mass flux variation, respectively.

$$\begin{aligned} Pr_{ij} &= -\overline{\rho} R_{jm} \tilde{U}_{i,m} - \overline{\rho} R_{im} \tilde{U}_{j,m}, \\ D_{ij} &= -(\overline{\rho u''_i u''_j u''_m} + \overline{p' u''_j} \delta_{im} + \overline{p' u''_i} \delta_{jm} - \overline{\tau''_{im} u''_j} - \overline{\tau''_{jm} u''_i})_{,m}, \\ P_{ij} &= \overline{p' (u''_{i,j} + u''_{j,i})} = P_{ij}^* + 2/3 \overline{p' u''_{k,k}} \delta_{ij}, \\ \varepsilon_{ij} &= \overline{\tau''_{im} u''_{j,m}} - \overline{\tau''_{jm} u''_{i,m}}, \\ V_{ij} &= -\overline{p}_{,j} \overline{u''_i} + -\overline{p}_{,i} \overline{u''_j} + \tilde{\tau}_{im,m} \overline{u''_j} + \tilde{\tau}_{jm,m} \overline{u''_i}. \end{aligned}$$

The turbulent dissipation in the compressible turbulence was proposed in [2,17], as follows:

$$\varepsilon = \varepsilon_s + \varepsilon_c \tag{5}$$

where, for homogeneous shear flow turbulence, $\overline{\rho} \varepsilon_s = \overline{\mu \omega'_i \omega'_i}$ (ω'_i is the fluctuating vorticity) and $\varepsilon_c = 4/3 \overline{\mu d^2}$ are the incompressible and dilatational (or compressible) parts of the turbulent dissipation rate, respectively. The authors argued that the incompressible part of the dissipation can be modeled by using the incompressible equation model [16], namely:

$$\frac{\partial}{\partial t} (\overline{\rho} \varepsilon_s) + \frac{\partial}{\partial x_k} (\overline{\rho} \varepsilon_s \tilde{U}_k) = \overline{\rho} \frac{\varepsilon_s}{K} (C_{\varepsilon 1} R_{km} \frac{\partial}{\partial x_m} \tilde{U}_k - C_{\varepsilon 2} \varepsilon_s) - \frac{\partial}{\partial x_k} (C_{\varepsilon 3} \overline{\rho} \frac{K}{\varepsilon_s} R_{km} \frac{\partial}{\partial x_m} \varepsilon_s) \tag{6}$$

4. Compressible Turbulence Model for the Pressure—Strain

Compressible turbulence modeling of the pressure-strain correlation is well known as an important problem in many interesting engineering applications related to environment, combustion flows, and hypersonic flights. During the last decade, different experiments and numerical simulations have been developed to understand the compressibility effects on pressure-strain. Despite the complexity of these problems, the last few years have been marked by an abundance of numerical results and a lot of advancement in second order closure. At first, researchers concentrated on the roles of the dilatational terms: pressure dilatation and the compressible part of the turbulent dissipation. In this context, Sarkar [3], Simone et al. [4], Hamba [5], and Blaisdell [18], using their DNS results, showed that the dilatational terms represent nearly 12% of turbulent kinetic energy production. They concluded that the notable decrease in the growth rate of the turbulent kinetic energy arising from compressibility was due to the inhibited turbulent production and not to the dilatational terms. In addition, these conclusions were confirmed by Adumitroaie et al. [11], Huang et al. [12], Goebel et al. [7], Foysi et al. [10], and Pantano et al. [9], who reported that the dilatational terms did not affect the compressible mixing layers. On the other hand, based on their research, they insisted that compressibility has a significant effect on the pressure-strain correlation via the pressure field. Consequently, the pressure-strain correlation requires a topic motivation in the second order model, which based on the

averaged Navier–Stokes (RANS) equations. Sarkar [3] performed two series of DNS, cases A1 to A4, for varying the initial gradient Mach number M_{g0} at a constant initial turbulent Mach number, $M_{t0} = 0.4$, and cases B1 to B3 for constant M_{g0} , ($M_{g0} = 0.22$) with varying M_{t0} . The reason behind the variety of DNS cases is to intercept the source changes in the turbulence structure at different compressibility levels, which are necessary for accurate modeling. The primary remarks coming from these DNS concern the behavior of the turbulent Mach number and the gradient Mach number in relation to the strong changes of the turbulent anisotropy. One can see that when the initial gradient Mach number is low, after an initial slight increase with the dimensionless time, $St(St \leq 5)$, and M_g shows a trend to become asymptotically constant, contrary to M_t , which grows constantly with St . In the case of A4, where it increases very highly, similar results are found for DNS [4]. Obviously, this gives a reason for several researchers, such as Huang et al. [12], Hamba [5], and Park et al. [19], to distinguish the DNS results [3] into three levels of compressibility: low, moderate, and high compressibility. In addition, the DNS results show that the behavior of M_g seems to be similar to the turbulence anisotropy, as it can be clearly seen for the shear stress anisotropy component b_{12} . Consequently, the authors concluded that M_g is an appropriate parameter to measure the strength of the structural compressibility, and it should be added to M_t in order to study the homogeneous highly sheared effects on the structural compressibility. So, a major challenge is to develop a model for the pressure-strain that is able to correctly capture the different compressibility levels. Thus, some compressible models have been derived for the pressure-strain correlation, most of which are derived from a simple extension of the incompressible LRR model [14], which reads as below:

$$P_{ij}^* = -C_1 \bar{\rho} \varepsilon_s b_{ij} + C_2 \bar{\rho} K (\tilde{S}_{ij} - \frac{1}{3} \tilde{S}_{ll} \delta_{ij}) + C_3 \bar{\rho} K [b_{ik} \tilde{S}_{jk} + b_{jk} \tilde{S}_{ik} - \frac{2}{3} b_{ml} \tilde{S}_{ml} \delta_{ij}] + C_4 \bar{\rho} K [b_{ik} \tilde{\Omega}_{jk} + b_{jk} \tilde{\Omega}_{ik}] \tag{7}$$

$$\tilde{S}_{ij} = 0.5(\tilde{U}_{i,j} + \tilde{U}_{j,i}), \tilde{\Omega}_{ij} = 0.5(\tilde{U}_{i,j} - \tilde{U}_{j,i}) \text{ and } b_{ij} = R_{ij}/2K - \delta_{ij}/3.$$

The coefficients models are: $C_1 = 3$, $C_2 = 0.8$, $C_3 = 1.75$ and $C_4 = 1.31$.

In this study, three compressible models for the pressure-strain correlation are considered. The models were developed by Adumitroaie et al. [11], Huang et al. [12], and Marzougui et al. [13]. The authors used different modeling approaches to modify the LRR incompressible model of the pressure-strain, making the coefficients C_i ($i = 1, 2, 3$, and 4) in Equation (7) a function of the turbulent Mach number, as seen in Table 1.

Table 1. Numerical coefficients of the pressure-strain model.

Model	C_1	C_2	C_3	C_4
Adumitroaie [11]	3	0.8	$1.75 + 0.15M_t$	$1.3 - 0.15M_t$
Huang [12]	3.6	0.8	$1.2 + 0.25 \exp(-0.05/M_t^3)$	$1.2 - 0.25 \exp(-0.05/M_t^3)$
Marzougui [13]	$3(1.0 - 0.8M_t^2)$	0.8	$1.75(1 - 1.4M_t^2)$	$1.31(1 - 0.5M_t)$

Adumitroaie et al. [11] derived a compressible model taking into account the compressibility effects. Their model for the pressure-strain is given by the following:

$$p_{ij}^* = -C_1 \bar{\rho} \varepsilon_s b_{ij} + (\frac{4}{5} + \frac{2}{5}d_1) \bar{\rho} K (\tilde{S}_{ij} - \frac{1}{3} \tilde{S}_{ll} \delta_{ij}) + 2\bar{\rho} K (1 - C_3 + 2d_2) [b_{ik} \tilde{S}_{jk} + b_{jk} \tilde{S}_{ik} - \frac{2}{3} b_{ml} \tilde{S}_{ml} \delta_{ij}] - \bar{\rho} K (1 - C_4 - 2d_2) [b_{ik} \tilde{\Omega}_{jk} + b_{jk} \tilde{\Omega}_{ik} - \frac{4}{3} d_2 \tilde{S}_{kk} b_{ij}] \tag{8}$$

The compressible coefficients d_1 and d_2 are determined from some compressible closures for the pressure-dilatation correlation. Here, we use the model of Sarkar et al. [2] to determine the coefficients $d_2 = 0.15M_t$ and $d_1 = 0$.

Huang et al. [12] assumed that the incompressible modeling approach of the pressure-strain can be used to develop turbulent models taking into account compressibility effects.

The authors used a damping function to modify the LRR model for the pressure-strain as follows:

$$P_{ij}^* = -C_1 \bar{\rho} \varepsilon_s b_{ij} + C_2 \bar{\rho} K (\tilde{S}_{ij} - \frac{1}{3} \tilde{S}_{ll} \delta_{ij}) + C_3 \bar{\rho} K [b_{ik} \tilde{S}_{jk} + b_{jk} \tilde{S}_{ik} - \frac{2}{3} b_{ml} \tilde{S}_{ml} \delta_{ij}] + C_4 \bar{\rho} K [b_{ik} \tilde{\Omega}_{jk} + b_{jk} \tilde{\Omega}_{ik}] \tag{9}$$

$$C_1 = 3.6, C_2 = 0.8, C_3 = 1.2 + 0.25 \exp(-0.05/M_t^3) \text{ and } C_4 = 1.2 - 0.25 \exp(-0.05/M_t^3).$$

Marzougui et al. [13] used the concept of the turbulent kinetic energy growth rate to introduce a compressibility correction on the LRR model coefficients [14], which became a polynomial functions of the turbulent Mach number.

$$P_{ij}^* = -C_1 \bar{\rho} \varepsilon_s b_{ij} + C_2 \bar{\rho} K (\tilde{S}_{ij} - \frac{1}{3} \tilde{S}_{ll} \delta_{ij}) + C_3 \bar{\rho} K [b_{ik} \tilde{S}_{jk} + b_{jk} \tilde{S}_{ik} - \frac{2}{3} b_{ml} \tilde{S}_{ml} \delta_{ij}] + C_4 \bar{\rho} K [b_{ik} \tilde{\Omega}_{jk} + b_{jk} \tilde{\Omega}_{ik}] \tag{10}$$

$$C_1 = 3 (1.0 - 0.8M_t^2), C_2 = 0.8, C_3 = 1.75 (1 - 1.4M_t^2) \text{ and } C_4 = 1.31 (1 - 0.5M_t).$$

The application of these models on compressible homogeneous shear flow has shown predictions that are in acceptable agreement with the DNS of Sarkar [3] for cases A1, A2 and A3, who did not report the case A4. Particularly, in this case, the model [13] predictions deviated excessively from the DNS results for all of the Reynolds stress anisotropy components, and the shear stress anisotropy b_{12} predictions were opposite to the DNS results. This can be attributed to the excessive reduction observed in the predicted behavior of the pressure-strain shear component. On the other hand, the model gave a high pressure-strain contribution in the normal stress anisotropy.

Proposal Model

The starting point of the proposed compressibility model is from some analyses and developments concerning the models developed by Adumitroaie et al. [11], Huang et al. [12], and Marzougui et al. [13]. They adopted different modeling approaches to modify the coefficients of the LRR model, which became a function of the turbulent Mach number (see Table 1). However, as can be seen, this modification is solely concerned with the coefficients C_3 and C_4 , which affect the polynomial linear term of the Reynolds stress anisotropy and the mean strain rate; the other coefficients, C_2 , which affects the mean strain rate, and C_1 of the return to isotropy model, are conserved as in the LRR model, without any compressibility correction. On the other hand, different analyses have been carried to show the influence of the pressure-strain on the Reynolds stress behavior. Hamba [5] presented a fine analysis for the compressible homogeneous shear flow case, and confirmed that the reduction of the transverse component P_{22} of the pressure-strain correlation principally caused the reduction of the transverse Reynolds stress R_{22} , which in turn induced a systematic reduction of the shear Reynolds stress, the streamwise component P_{11} of the pressure-strain, and then the growth rate of the turbulent kinetic energy. Thus, the compressibility correction of the coefficients C_3 and C_4 seem to be sufficient to capture compressibility effects. In this context, according to Park et al. [18] and Huang et al. [12], in addition to the compressibility correction of the coefficients C_3 and C_4 , the coefficient C_2 should be corrected with compressible parameters, such as M_t and M_g , or others. One can see that C_2 directly affects the shear component P_{12} of the pressure-strain, which has an evident contribution in the transport equation for the Reynolds shear stress, R_{12} . On the other hand, the reduction of P_{12} , which works as a sink term in the transport equation for R_{12} , leads to an increase in the growth rate of the turbulent kinetic energy via the growth of R_{12} . This is not suitable using model. So, more attention should be paid to the modeling for P_{12} . Khlifi et al. [20] considered an equation of the dilatation fluctuation to modify the incompressible C_2 and the return to isotropy C_1 -coefficients [14], as follows:

$$C_2 = 0.8(1 + 0.45M_t^4) \exp(-0.015M_g), \tag{11}$$

$$C_1 = 3(10.7M_t^2) \tag{12}$$

This is the first point on which the present study is based in order to revise the previous models. For this revision, the Khlifi et al. [20] model was chosen to modify the C_1 and C_2 coefficients in [11–13]. The reason behind this choice is that model [20] involves M_t and M_g , as suggested by different studies cited previously, and it is linked to M_t^4 to distinguish between low- M_t and high- M_t regimes. Thus, all of the coefficients of models [11–13] are expressed as a function of the turbulent Mach number and the gradient Mach number. Considering Equations (11) and (12), the proposal coefficients models are summarized in Table 2.

Table 2. Numerical coefficients of the pressure-strain model.

Model	C_1	C_2	C_3	C_4
Adumitroaie modified	$3(1.0 - 0.7M_t^2)$	$0.8(1 + 0.45M_t^4)e^{-0.015M_g}$	$1.75 + 0.15M_t$	$1.3 - 0.15M_t$
Huang modified	$3(1.0 - 0.7M_t^2)$	$0.8(1 + 0.45M_t^4)e^{-0.015M_g}$	$1.2 + 0.25e^{-0.05M_t}$	$1.2 - 0.25e^{-0.05M_t}$
Marzougui modified	$3(1.0 - 0.7M_t^2)$	$0.8(1 + 0.45M_t^4)e^{-0.015M_g}$	$C_3 = 1.75(1 - 1.4M_t^2)$	$C_4 = 1.31(1 - 0.5M_t)$

5. Applications

5.1. Simulation of Compressible Homogeneous Shear Flow

For compressible homogeneous shear flow, the mean velocity gradient is given by the following:

$$\tilde{U}_{ij} = S\delta_{i1}\delta_{j2} \tag{13}$$

For homogeneous shear flow, $\bar{p} = cte$ and $\tilde{T} = \tilde{T}(t)$ is related to the Reynolds-average of the pressure using the state equation for ideal gas:

$$\bar{P} = \bar{p}R\tilde{T} \tag{14}$$

The Favre averaged basic second order model equations are as follows:

$$\bar{\rho} \frac{d}{dt} R_{ij} = Pr_{ij} + P_{ij}^* - \frac{2}{3}\bar{\rho}(\epsilon_s + \epsilon_c)\delta_{ij} + \frac{2}{3}\overline{p'd'}\delta_{ij} \tag{15}$$

$$\bar{\rho} \frac{d}{dt} \epsilon_s = C_{\epsilon 1}\bar{\rho} \frac{\epsilon_s}{K} R_{km} \frac{\partial}{\partial x_m} \tilde{U}_k - C_{\epsilon 2}\bar{\rho} \frac{\epsilon_s^2}{K} \tag{16}$$

Assuming that the mean specific heat is constant, the equivalently temperature equation for the Reynolds averaged energy may be written in a simplified form [21], namely:

$$\bar{\rho} \bar{C}_v \frac{d}{dt} \tilde{T} = \bar{p}(\epsilon_s + \epsilon_c) - \pi_d \tag{17}$$

Contraction $i = j$ in Equation (12) leads to an equation for the Favre-averaged turbulent kinetic energy, $K = 0.5\bar{\rho}u_i''u_i''/\bar{\rho}$, as follows:

$$\bar{\rho} \frac{d}{dt} K = P - \bar{p}(\epsilon_s + \epsilon_c) + \overline{p'd'} \tag{18}$$

where $P = -\bar{\rho}R_{ij}\tilde{U}_{ij}$ is the turbulent production.

The transport equation for the turbulent Mach number, $M_t = \sqrt{2K/\gamma R\tilde{T}}$, can be obtained from combining Equations (17) and (18) as follows [21]:

$$\frac{d}{dt} M_t = \frac{M_t}{2\bar{\rho}K} (1 + 0.5\gamma(\gamma - 1)M_t^2)(\overline{p'd'} - \bar{p}\epsilon) + \frac{M_t}{2K} P \tag{19}$$

where $\gamma = c_p/c_v$.

5.2. Simulation of Compressible Mixing Layers

The flow is governed by the averaged Navier-Stokes equations associated with those that describe the energy, Reynolds stress, and turbulent dissipation. The simplest resulting continuity, momentum, and energy equation for stationary mixing layers can be written as follows [16]:

$$\frac{\partial}{\partial x_i} \bar{\rho} \tilde{U}_i = 0, \tag{20}$$

$$\frac{\partial}{\partial x_i} (\bar{\rho} \tilde{U}_i \tilde{U}_j) = - \frac{\partial}{\partial x_j} (\overline{\rho u_i'' u_j''}), \tag{21}$$

$$\frac{\partial}{\partial x_j} (\bar{\rho} C_v \tilde{T} \tilde{U}_j) = - \frac{\partial}{\partial x_j} (C_v \overline{\rho u_j'' T''}) + \bar{\rho} (\varepsilon_s + \varepsilon_c) - \overline{p' u'_{i,i}}. \tag{22}$$

The Reynolds stress is the solution of the follow equation

$$\frac{\partial}{\partial x_m} (\bar{\rho} \tilde{U}_m R_{ij}) = - (R_{im} \tilde{U}_{j,m} + R_{jm} \tilde{U}_{i,m}) + \frac{\partial}{\partial x_m} (\overline{\rho u_i'' u_j'' u_m''}) + \varphi_{ij}^* + \frac{2}{3} \overline{p' u'_{i,i}} \delta_{ij} - \frac{2}{3} \varepsilon \delta_{ij}. \tag{23}$$

The turbulent solenoidal dissipation rate shall is calculated from the classical model equation, namely:

$$\frac{\partial}{\partial x_k} (\bar{\rho} \varepsilon_s \tilde{U}_k) = \bar{\rho} \frac{\varepsilon_s}{K} (C_{\varepsilon 1} R_{km} \frac{\partial}{\partial x_m} \tilde{U}_k - C_{\varepsilon 2} \varepsilon_s) - \frac{\partial}{\partial x_k} (C_{\varepsilon 3} \bar{\rho} \frac{K}{\varepsilon_s} R_{km} \frac{\partial}{\partial x_m} \varepsilon_s). \tag{24}$$

In the above mentioned transport equations, different terms should be modeled, and the gradient diffusion hypothesis is used to represent the following:

- The turbulent heat flux [16]:

$$\overline{\rho u_i'' T''} = -C_T \frac{K}{\varepsilon} \overline{\rho u_i'' u_m''} \frac{\partial}{\partial x_m} \tilde{T}. \tag{25}$$

- The diffusion term [16]

$$\overline{\rho u_i'' u_j'' u_m''} = -C_s \frac{K}{\rho \varepsilon} \overline{\rho u_i'' u_m''} \frac{\partial}{\partial x_m} \overline{\rho u_j'' u_m''}. \tag{26}$$

6. Results and Discussion

The ability of the models of Adumitroaie et al. [11], Huang et al. [12], and Marzougui et al. [13] models, as well as their proposal modified forms, called the Adumitroaie modified, Huang modified, and Marzougui modified models, respectively, for the pressure-strain correlation (see Tables 1 and 2), in order to predict compressible homogeneous turbulent shear and planar mixing layer turbulent flows will now be considered.

6.1. Homogeneous Shear Flow

The averaged transport for compressible homogeneous turbulence, given by Equations (15)–(19), is solved numerically using a fourth-order Runge–Kutta numerical scheme. Figures presented in this paper show the comparisons between the predictions obtained by the proposed models, called the Adumitroaie modified, Huang modified, and Marzougui modified models, and those from their corresponding original models, developed by Adumitroaie et al. [11], Huang et al. [12], and Marzougui et al. [13], respectively, and with the DNS results [3]. The reason for considering various models tests is to verify the proposal modifications validation and its added value in the prediction of the compressibility effects; especially when the proposed corrections are applied to three models build on different approaches, as shown in the indicated Section 4. In the same context, the DNS results considered here correspond to the different initial conditions listed in Table 3, from a low compressibility in case A1, to case A4, for which the compressibility is higher. From all of the figures, it is clear that both models provide a qualitative performance to reproduce

the DNS results for all cases. However, one can see the accuracy of the proposal models for the prediction of the major characteristic parameters for compressible homogeneous shear flow, which can be expected from the model's revision.

Table 3. Initial conditions for homogeneous shear flow: DNS [3].

Case	M_{t0}	$(\varepsilon_s/SK)_0$	M_{g0}	b_{11}	b_{22}	b_{12}
A1	0.4	1.8	0.22	0	0	0
A2	0.4	3.6	0.44	0	0	0
A3	0.4	5.4	0.66	0	0	0
A4	0.4	10.8	1.32	0	0	0
B1	0.13	5.4	0.22	0	0	0
B2	0.2	3.6	0.22	0	0	0
B3	0.4	1.8	0.22	0	0	0

Figure 1 shows the normalized dissipation ε_{sk} ($\varepsilon_{sk} = \varepsilon_s/SK$) for cases A1 to A4 from DNS [3]. The results show that the proposal models better predict the trend of the decrease of ε_s/SK when M_{g0} increases, as compressibility effects cause a significant reduction in the turbulent production from numerical simulation cases A1 to A4. In fact, $(\varepsilon_s/SK = -2b_{12}(\varepsilon_s/P))$, according to DNS [3], (ε_s/P) appeared to be insensitive to compressibility effects and showed little differences between cases A1 to A4. This implies that the strong reduction in the shear stress anisotropy, b_{12} , is responsible for the lowered gradient Mach number increases.

Figure 2 presents the behavior of the turbulent Mach number for cases A1 to A4. It is clearly seen that for both models, the original models and their modified versions are similar in their prediction of the correct trend of, an increase with creasing initial M_{g0} for little dimensionless time ($St \leq 5$). For ($St \geq 10$), the difference between both models predictions are smaller in cases A1 and A2. On the other hand, in case A3 and particularly in case A4, the models become different; this can be seen in Figure 2d, which corresponds to case A4. One can see that the modified models predict the asymptotic trend of M_t better than the original models.

Figures 3–5 show the non-dimensional time St variation of the Reynolds stress anisotropies of b_{11} , b_{12} , and b_{22} , respectively, for cases A1 to A4. For case A1, which corresponds to low compressibility, the results are shown in Figures 3a, 4a and 5a, with both models being nearly similar, and the difference between their predictions being smaller. The models provide an acceptable performance for reproducing the DNS [3] results of this case. The results for case A2 and A3 are shown in Figures 3b,c, 4b,c and 5b,c. The Adumitroaie et al. [11] and Huang et al. [12] models appear to be insensitive to the increase of the streamwise b_{11} and the transverse b_{22} of the Reynolds stress anisotropies when the compressibility increases; the models' results are in disagreement with the DNS data. However, these models have an acceptable performance for the prediction of the correct behavior of the reduced shear stress anisotropy b_{12} . For the Marzougui et al. [13] model, the results are in good agreement with the DNS data, the model predicts the asymptotic behaviors of the shear stress anisotropy and the normal components b_{11} and b_{22} well.

Figures 3d, 4d and 5d show the result predictions for case A4, which corresponds to a high compressibility. The DNS data show that there is a strong amplification of energy arising from the compressibility and then the normal stress components become stronger. The Adumitroaie et al. [11] and Huang et al. [12] models predicted the same anisotropy levels as in previous cases; these models were still unable to predict the changes in the magnitude of the normal Reynolds stress anisotropy when the compressibility was higher. As can be seen in the previous figures, the models [11,12] appear to be insensitive to the increase of the streamwise b_{11} and the transverse b_{22} Reynolds stress anisotropies when the compressibility increases. However, these models are in qualitative agreement with the DNS data for the shear stress anisotropy b_{12} .

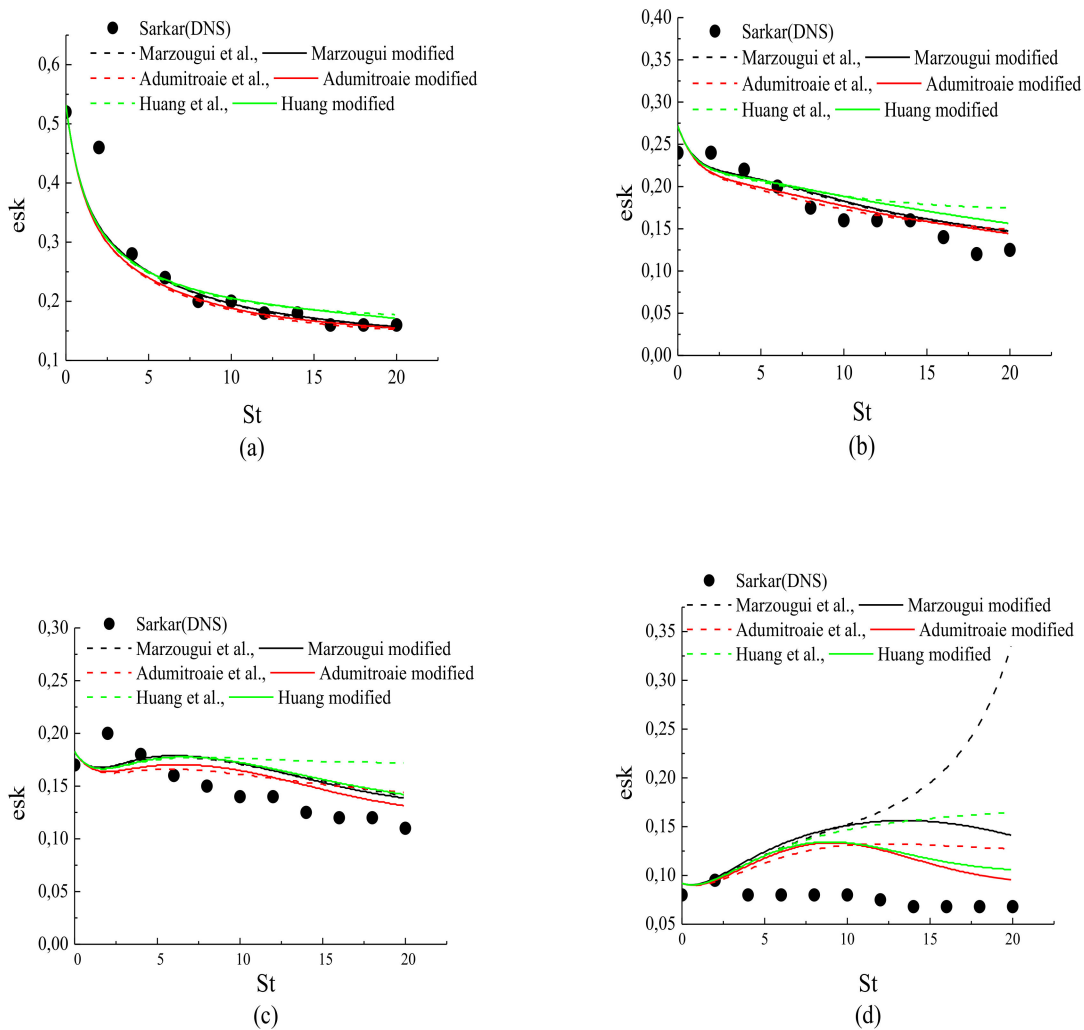


Figure 1. Time evolution of the normalized dissipation, ($esk = \varepsilon_s/SK$ in the following cases: (a) A1; (b) A2; (c) A3; (d) A4.

The Marzougui et al. [13] model predictions deviated from the DNS data for the all of the Reynolds stress anisotropies components. The authors attributed the deficiency of their model to the fact that A4 falls within the rapid distortion limited for which the non-linear effects of the pressure-strain are unimportant, and they recommend an eventual revision of the model; this is what has been investigated by Khelifi et al. [20]. On the other hand, from Figures 3–5, one can see the improvements brought about by the proposed modifications of the existent models [11–13] for the pressure-strain correlation in the prediction of the changes in the magnitude of the compressible Reynolds stress anisotropies. The modified models give results for the normal components b_{11} and b_{22} , which are in reasonable agreement with the DNS data and predict the asymptotic shear stress anisotropy well for all cases.

Figures 6–8 present the behavior of the pressure-strain correlation $P_{ij} = P^*_{ij}/2SK$, ($i, j = 1, 2$) for cases A1 to A4 from DNS [3]. The results for case A1 are shown in Figures 6a, 7a and 8a; all of the models are in qualitative acceptable agreement with the DNS results. The results for cases A2 to A4 are shown in Figures 6b–d, 7b–d and 8b–d; the modified models yielded reasonable agreement with the DNS data, and clearly predicted the reduced pressure-strain components better than their original versions. This was concluded from the DNS results [3,4], in which it is argued that the pressure fluctuations and all components of the pressure-strain correlation showed a monotone decrease with the increasing gradient Mach number.

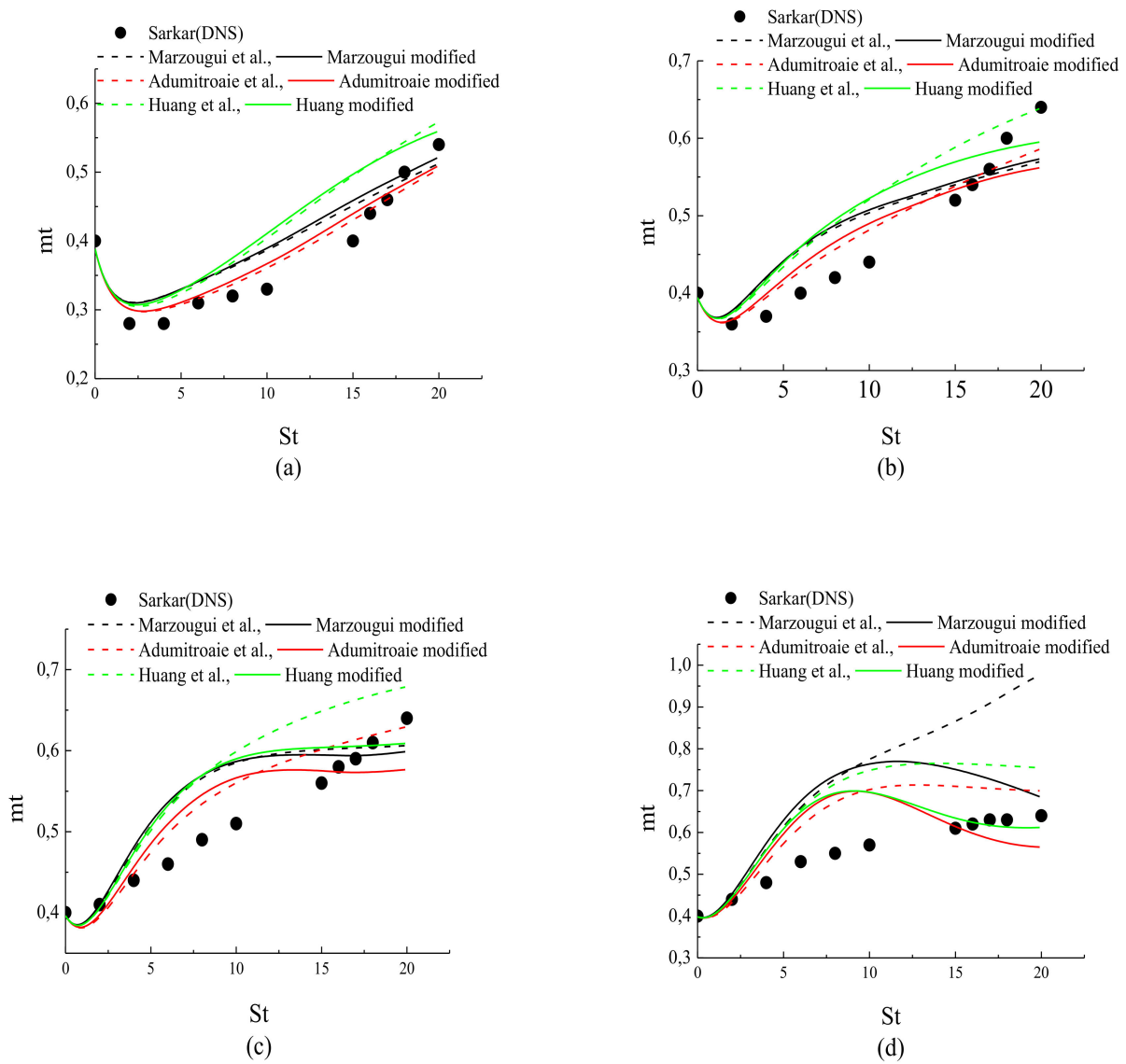


Figure 2. Time evolution of the turbulent Mach number, in the following cases: (a) A1; (b) A2; (c) A3; (d) A4.

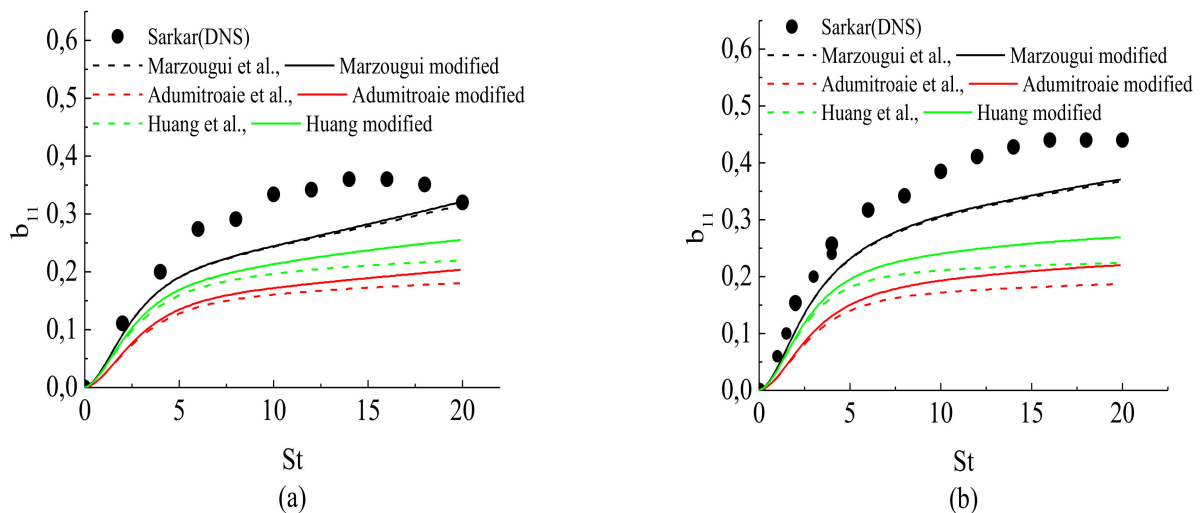


Figure 3. Cont.

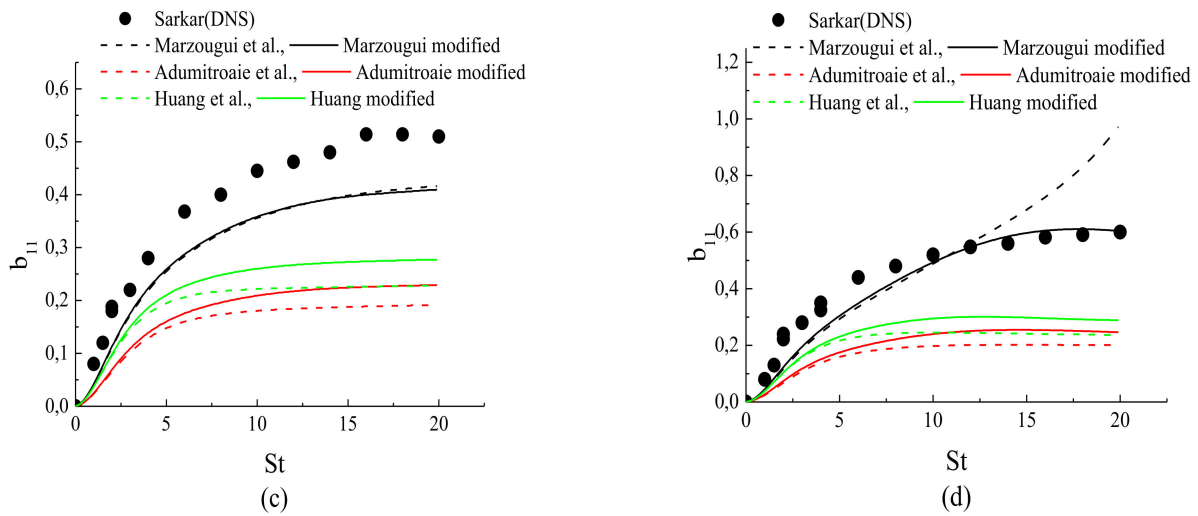


Figure 3. Time evolution of the streamwise Reynolds stress anisotropy, in the following cases: (a) 1; (b) A2; (c) A3; (d) A4.

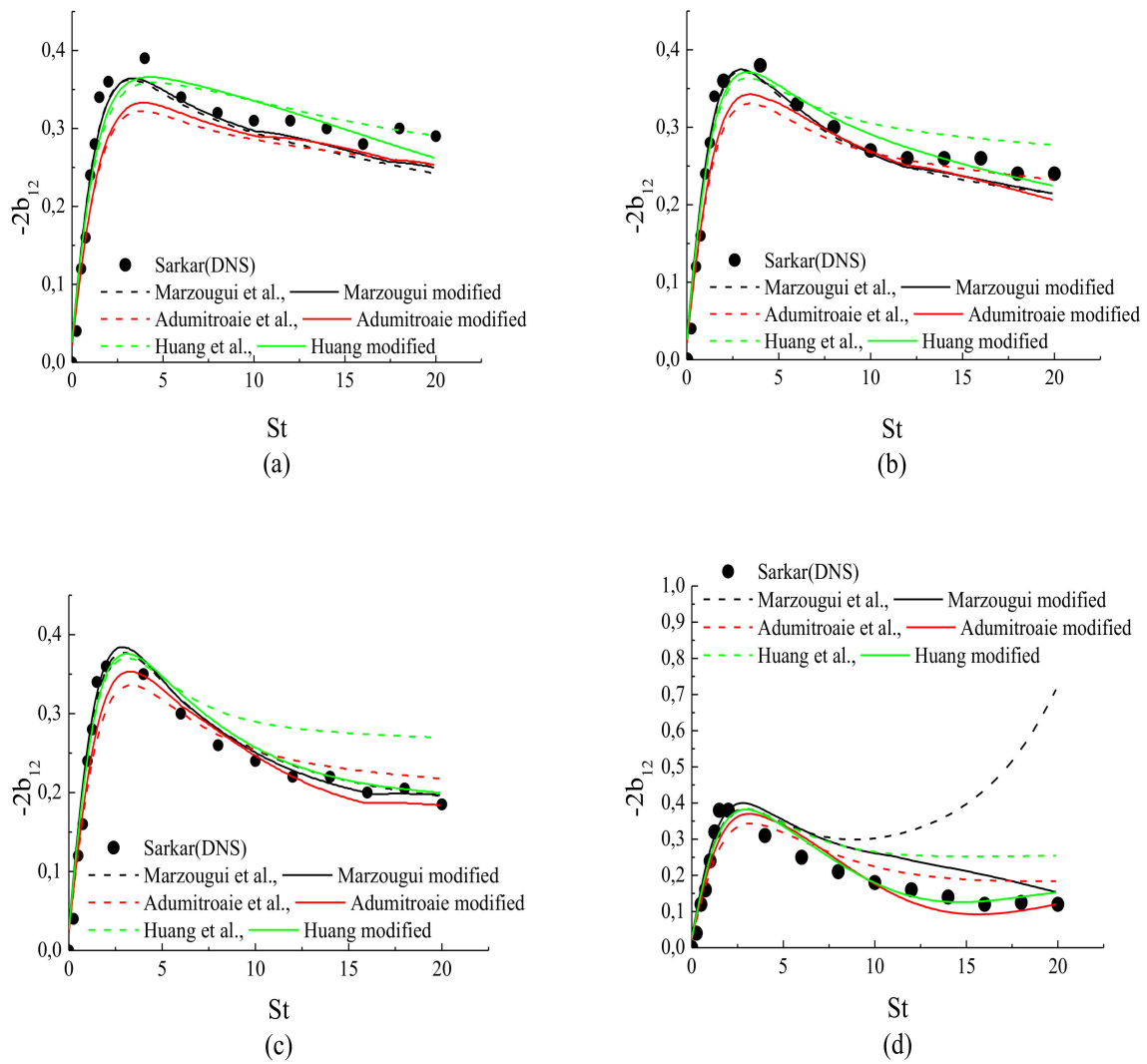


Figure 4. Time evolution of the shear Reynolds stress anisotropy, b_{12} , in the following cases: (a) A1; (b) A2; (c) A3; (d) A4.

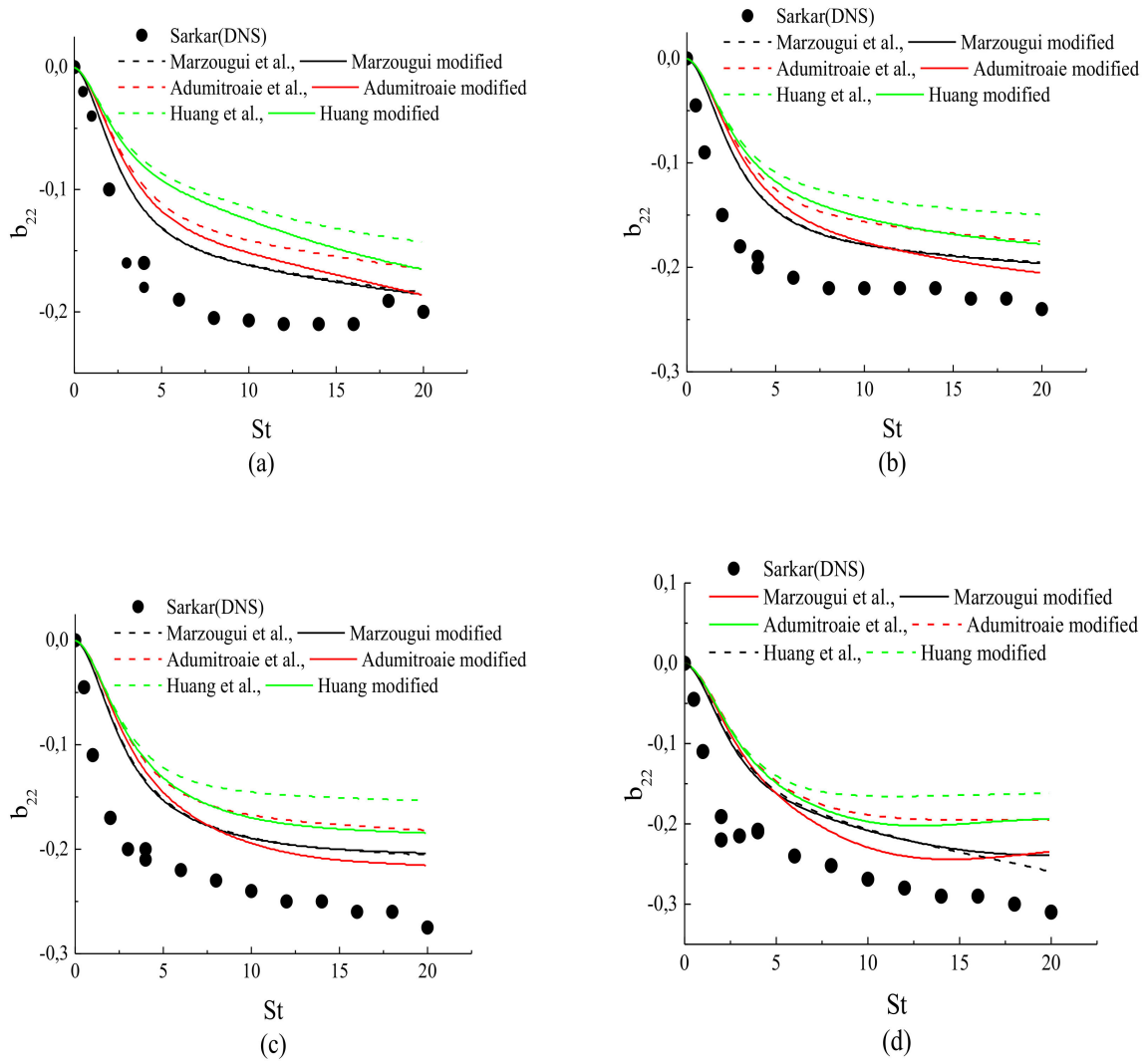


Figure 5. Time evolution of the transverse Reynolds stress anisotropy, in the following cases: (a) A1; (b) A2; (c) A3; (d) A4.

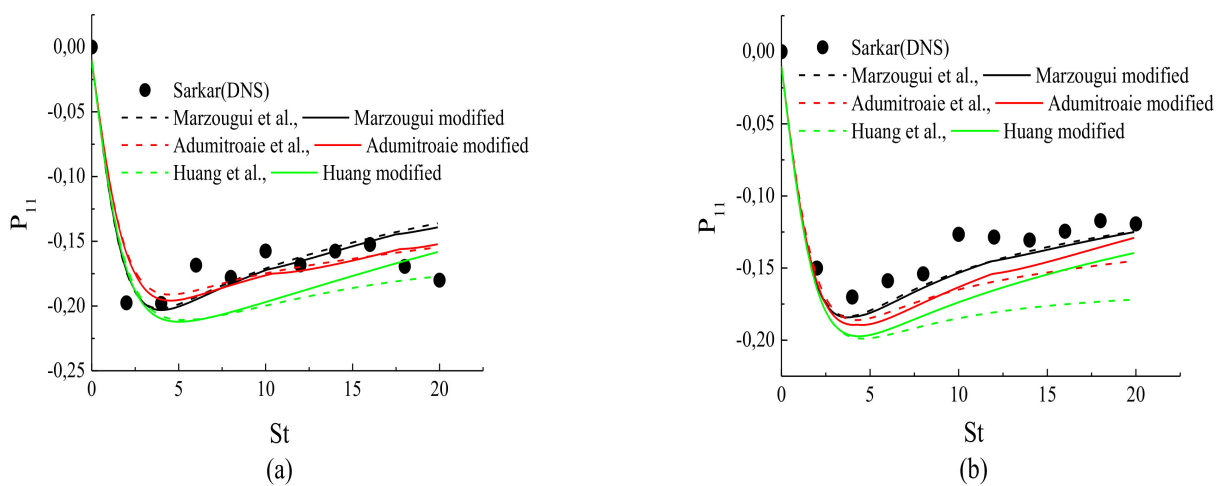


Figure 6. Cont.

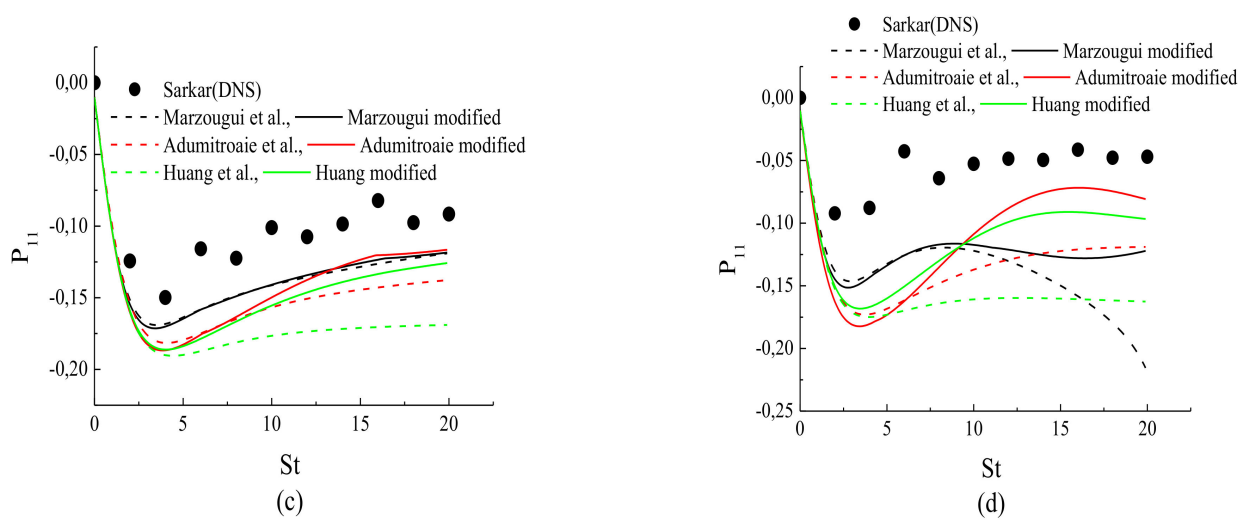


Figure 6. Time evolution of the pressure-strain component, in the following cases: (a) A1; (b) A2; (c) A3; (d) A4.

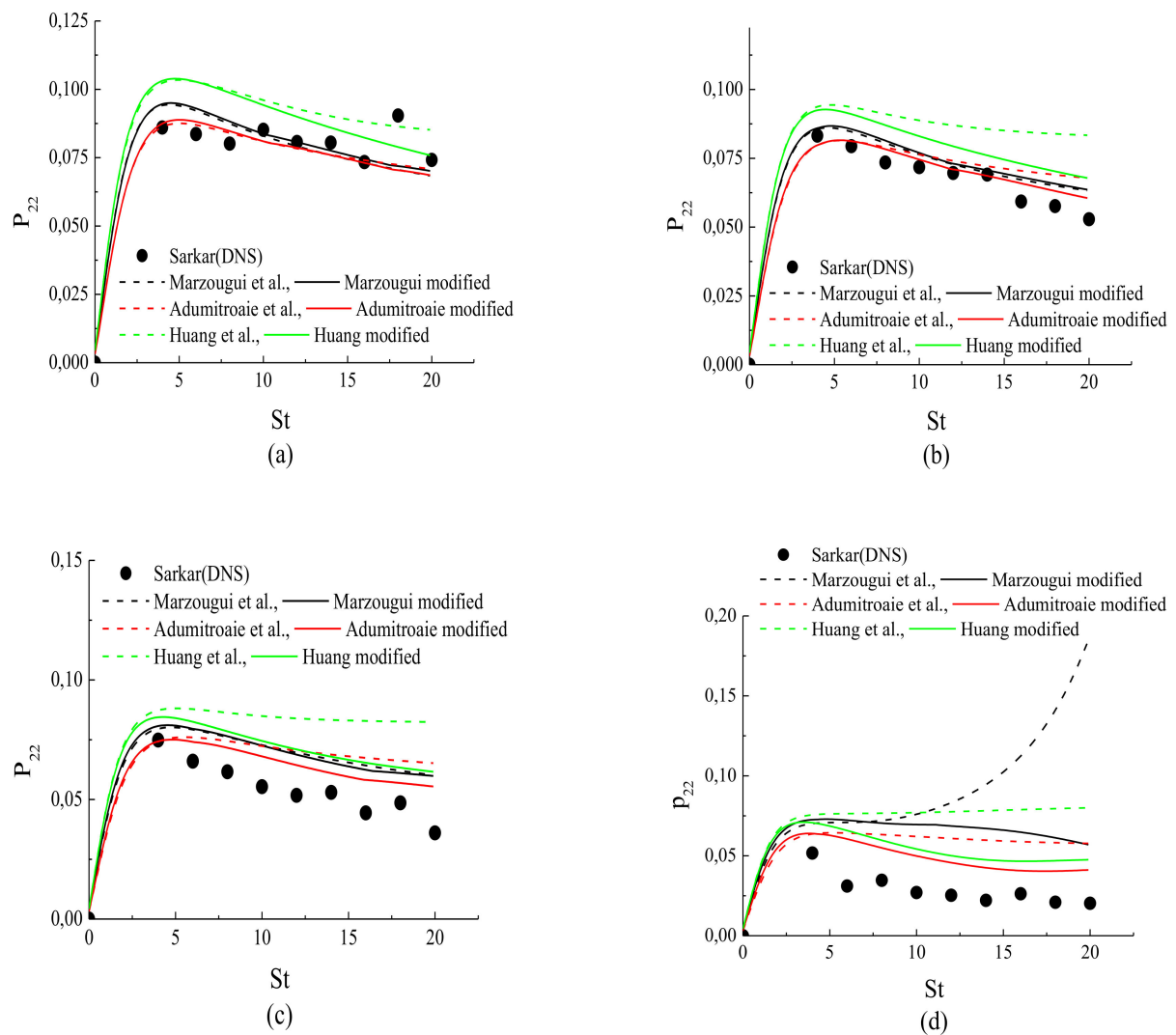


Figure 7. Time evolution of the pressure-strain component, P_{22} in the following cases: (a) A1; (b) A2; (c) A3; (d) A4.

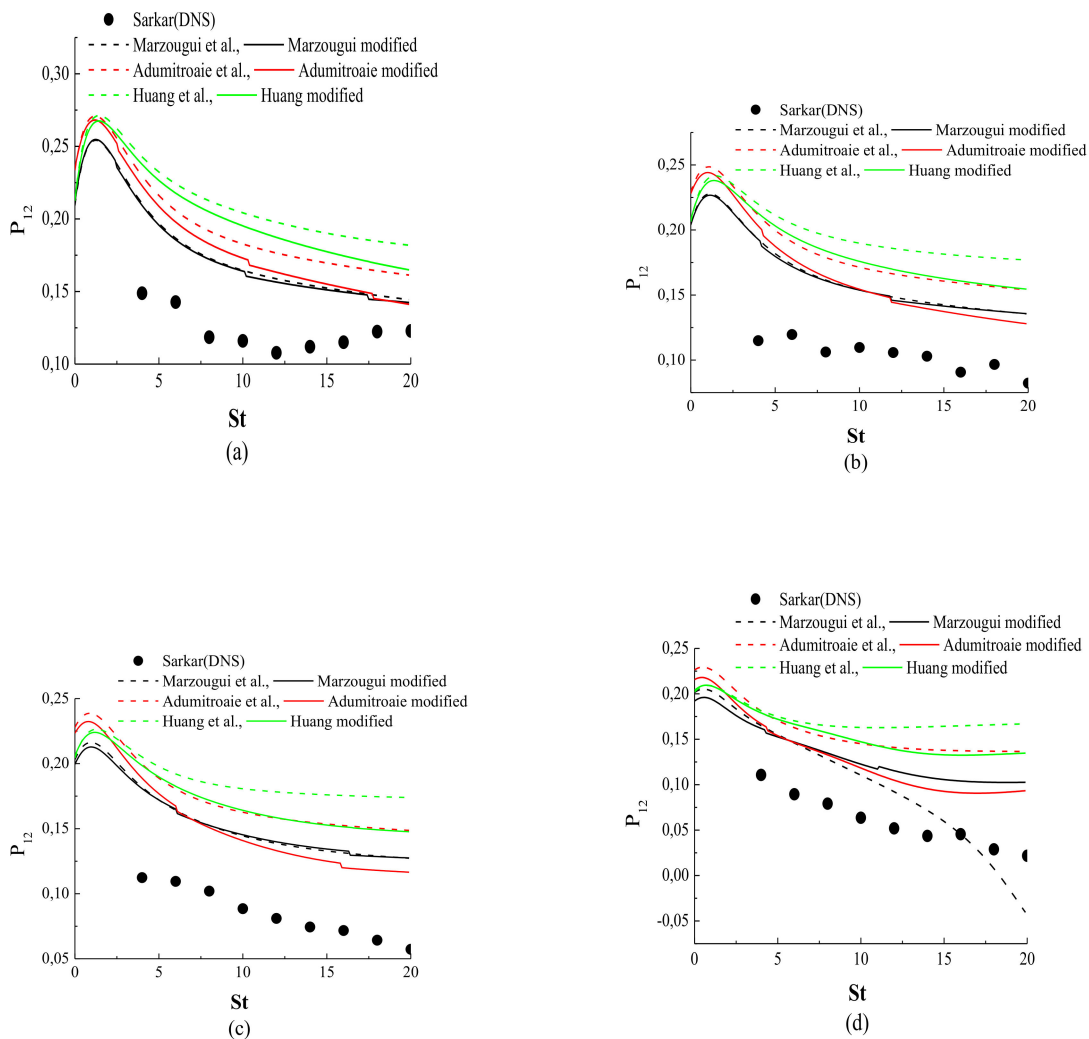


Figure 8. Time evolution of the pressure-strain component in the following cases: (a) A1, (b) A2; (c) A3; (d) A4.

6.2. Mixing Layers

In this study, the computation of two free streams of a fully developed compressible mixing layer (see Figure 9) is examined. The flows are characterized typically by the parameters $s = \rho_2 / \rho_1$ and $r = U_2 / U_1$, which are the density and velocity ratios, respectively. The experiment conditions of Goebel et al. [7] are listed in Table 4.

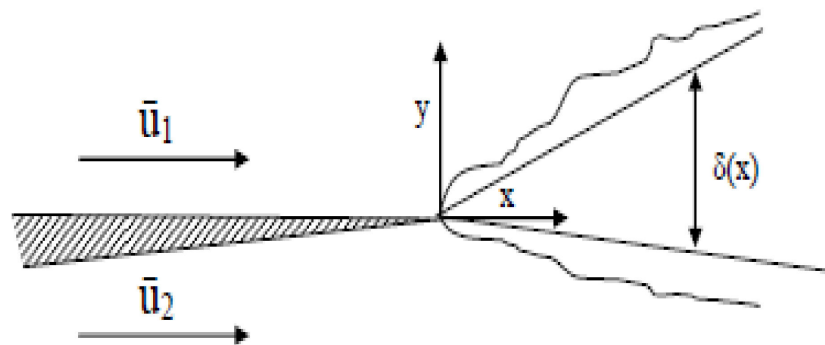


Figure 9. Turbulent mixing layer.

Table 4. Experiment of Goebel and Dutton.

M_c	$r = \frac{U_2}{U_1}$	$s = \frac{\rho_2}{\rho_1}$
0.2	0.76	0.78
0.46	0	0
0.69	0	0
0.86	0.16	0.6

The basic Equations (20)–(26) on which the second order model for the stationary compressible mixing layers is based are solved using a finite difference scheme. The grid of the computational physical domain, which is a rectangular box defined by the set of point (x, y) , has 6666×41 points. The initial profiles for $\varepsilon_s, \bar{\rho}$ and, \tilde{T} which are not available in the experiment of Goebel et al. [7], are generated as follows:

- The initial profile of the turbulent dissipation is determined from the turbulent viscosity model.

$$\varepsilon_s = -C_\mu \bar{\rho} \frac{K^2}{\rho u'' v''} \frac{\partial}{\partial y} \tilde{U} C_\mu = 0.09, \tag{27}$$

- The initial profile of the temperature is obtained from the following similarity

$$\frac{\tilde{U} - U_2}{(U_1 - U_2)} = \frac{\tilde{T} - T_2}{(T_1 - T_2)}, \tag{28}$$

- The state equation of perfect gas is used to determine the initial profile of the density. The values of the constant models used in the present simulation are as follows:

$$C_{\varepsilon 1} = 1.4, C_{\varepsilon 2} = 1.8, C_\mu = 0.09, C_\varepsilon = 0.25, C_T = 0.26.$$

According to Sarkar [3], homogeneous shear flow is closely related to the mixing layers, this allows Mg to be connected to M_c . Thus, according to Khlifi et al. [20], the coefficients C_i of the Adumitroaie et al. [11] model are expressed as a function of the turbulent Mach number and the convective Mach number, as shown in Table 5.

Table 5. Numerical coefficients of the pressure-strain model.

Model	C_1	C_2	C_3	C_4
Adumitroaie modified	$3(1.0 - 2.5M_t^2)$	$0.8(1 + 4.5M_t^4) \exp(-0.00022Mc)$	$1.75 + 0.15M_t$	$1.3 - 0.15M_t$

In this work, the simulation was limited to the Adumitroaie et al. [11] and Adumitroaie modified (referred to presently) models, as listed in Tables 1 and 5. Figures 10–13 compare the computed results from the Adumitroaie et al. model and the present models with the experiments of Goebel et al. [7] for three cases: $M_c = 0.2, M_c = 0.69,$ and $M_c = 0.86,$ for which the important characteristic parameter of the developed planar mixing layers is represented in relation to the similarity variable $y^* = (y - y_c)/\delta,$ where y is the local cross stream coordinate and y_c is the cross-stream coordinate corresponding to $U^* = 0.5.$ The normalized stream mean velocity $U^* = (\tilde{U} - U_2)/(U_1 - U_2),$ is plotted in Figure 10, the calculated profiles for both of the two models are in good agreement with the experiment results for a low convective Mach number $M_c = 0.2,$ and the largest convective Mach number $M_c = 0.86,$ as shown in Figure 10a,b, respectively. The expected effects of the two Mach numbers M_t and M_c on the changes in pressure-strain correlation are clearly seen in Figures 11–13, which compare the Reynolds similarity intensity profiles as follows: the streamwise intensity $R11 = \sqrt{\rho u''^2} / \bar{\rho} (U_1 - U_2)^2,$ the transverse intensity

$R_{22} = \sqrt{\overline{\rho v''^2}} / \bar{\rho}(U_1 - U_2)^2$, and the shear stress $R_{12} = \overline{\rho u''^2 v''^2} / \bar{\rho}(U_1 - U_2)^2$ obtained by the present model and by Adumitroaie et al. [11] model with the experiment results of Goebel et al. [7]. The two models have nearly similar behaviors for small values of convective Mach numbers ($M_c = 0.2$), as observed in Figures 11a,b, 12a,b and 13a,b. When the compressibility is more significant, $M_c = 0.86$, Figures 11c, 12c and 13c show that the present model results are in reasonable agreement with the experiment data compared with those obtained by the Adumitroaie et al. [11]. The compressibility effects via the M_c -influence on the mixing layers anisotropy can be more clearly seen in Figure 14, which compares the variation of the maximum values of the Reynolds intensities: $(R_{11})_{max}$, $(R_{22})_{max}$, and $(R_{12})_{max}$ versus the convective Mach number with different experiment and DNS data [7,9,10]. We found that the present model better predicts the decrease in the maximum values of all Reynolds stress intensities with increasing the initial value of M_c . However, the influence of M_c on the variation of $(R_{11})_{max}$ is not significant (Figure 14a) as can be seen for the other components in Figure 14b,c. This behavior can be found in the analysis of [19], who concluded that the reduction of the pressure-strain directly caused a reduction of R_{22} . However, the reduction of R_{11} involved turbulent production and the pressure-strain terms.

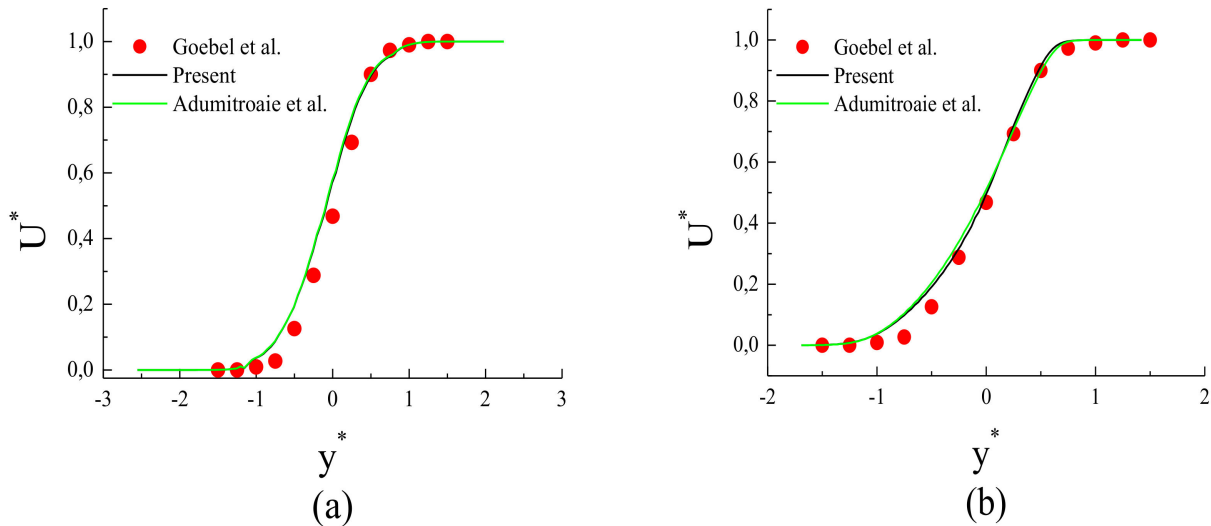


Figure 10. Similarity profiles of the mean velocity, in the following cases: (a,b).

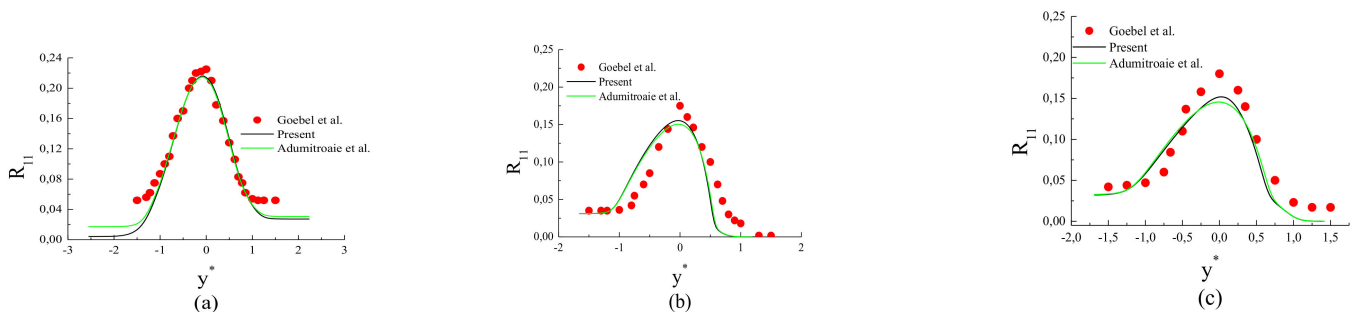


Figure 11. Similarity profiles of R_{11} in the cases: (a) $M_c = 0.2$, (b) $M_c = 0.69$, and (c) $M_c = 0.86$.

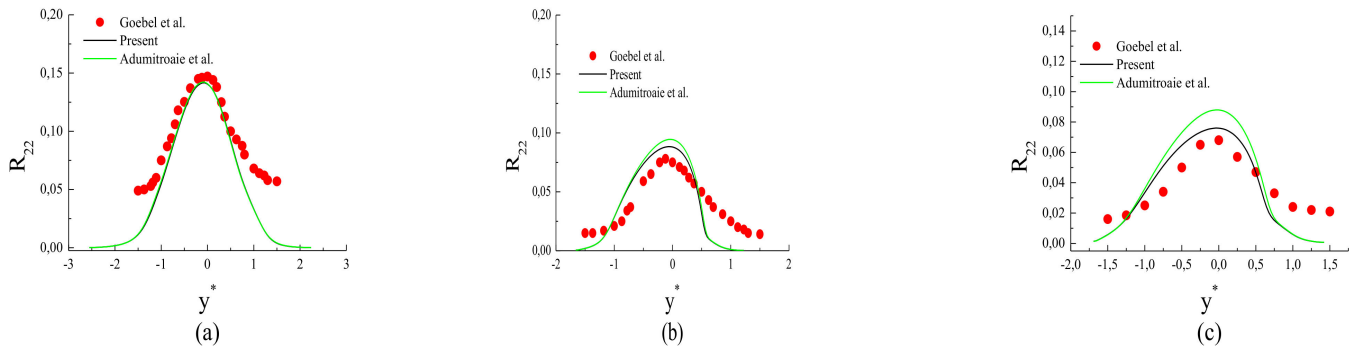


Figure 12. Similarity profiles of in the cases: (a–c).

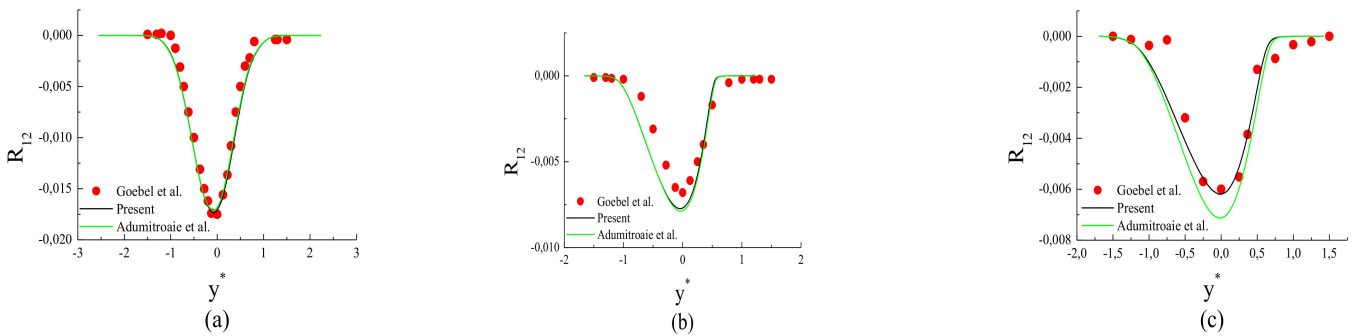


Figure 13. Similarity profiles of R_{12} in the cases: (a) $M_c = 0.2$, (b) $M_c = 0.69$, and (c) $M_c = 0.86$.

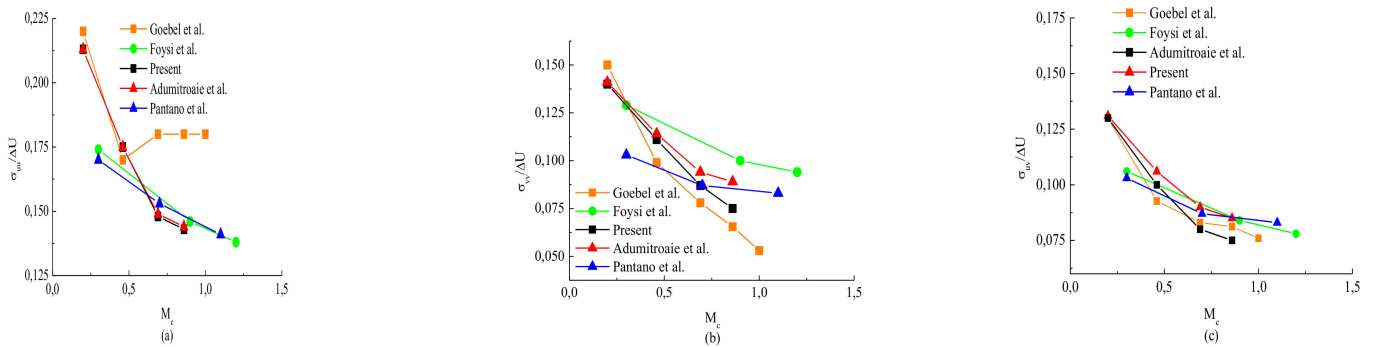


Figure 14. The influence of the convective Mach number on the maximum Reynolds stress: (a) $(R_{11})_{max}$, (b) $(R_{22})_{max}$ and, (c) $(R_{12})_{max}$.

Figure 15 compares the centerline values of the Reynolds stress anisotropy components: $(b_{11})_{max}$, $(b_{22})_{max}$ and $(b_{12})_{max}$ versus convective Mach number computed by the present model and those given by Adumitroaie et al. model with the DNS datas of Freund et al. [22]. It is found that the present model predicts the decreasing trend of shear stress anisotropy b_{12} and the increasing trend of all the normal stress anisotropies b_{11} and b_{22} with increasing convective Mach number well. The Adumitroaie et al. model shows that such trends occurred, but incorrectly followed the DNS data; thus, the peaks of b_{ij} were not relatively affected by M_c . This gives reason to imply M_c in addition to M_t for the eventual modeling of the pressure-strain correlation, which controls the anisotropy changes arising from the compressibility effects. Regarding Figure 14a, one can remark that both models give nearly similar peaks for R_{11} , which decrease less than the other components R_{22} and R_{12} when increasing M_c . This leads to a monotone increase of all the normal stress anisotropies with M_c , as can be seen in Figure 15a,c; this behavior was found by the DNS of Vreman et al. [6] and Freund et al. [22]. Obviously, this act comes from

compressibility via a reduction in the magnitude of all components of the pressure-strain correlation with M_c .

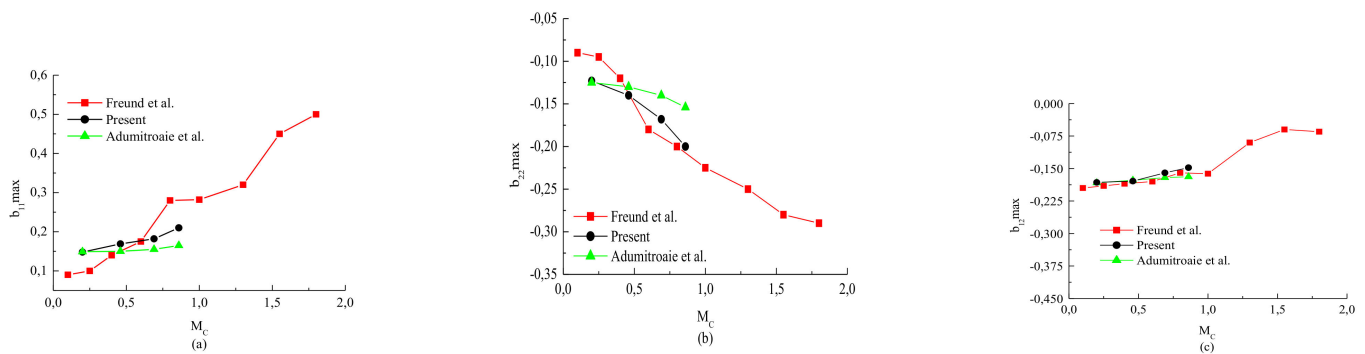


Figure 15. The influence of the convective Mach number on the maximum Reynolds stress anisotropies: (a) $(b_{11})_{\max}$, (b) $(b_{22})_{\max}$, and (c) $(b_{12})_{\max}$.

From the previous results, one can conclude that the pressure-strain closure involving the parameter M_g appears to be suited to study compressibility effects on highly sheared homogeneous turbulence. In addition, the convective Mach number M_c seems to be an appropriate parameter to study such effects on mixing layers. There are differences in the accuracy between the models in the prediction compressibility effects on homogeneous shear flow and mixing layers. These differences can be attributed to the modeling approaches on which the previous models are built.

7. Conclusions

In this study, the Favre Reynolds stress model is used for the prediction compressibility effects in two important turbulent flow cases—homogeneous shear flow and the spatially planar mixing layers. Evaluation of the density extension turbulence models of Adumitroaie et al. [11], Huang et al. [12], and Marzougui et al. [13] for the pressure-strain correlation were examined. A revision of these models by considering the Khlifi et al. [20] model, lead to expressing all of the coefficients models [11–13] in function of the gradient and convective Mach numbers, in addition to the turbulent Mach number. The application of the proposed models referred to as Adumitroaie modified, Huang modified, and Marzougui modified models, to predict the previous flows shows satisfactory agreement with the available DNS data and the experiment results. The proposed models appear to be able to accurately predict the structural compressibility effects on homogeneous shear flow as a significant decrease in the magnitude of the Reynolds shear stress and a reduction in the pressure-strain components with increasing initial values of the gradient Mach number. In addition, the proposed model, referred to as the Adumitroaie modified model, successfully predicted the changes in the similarity of the Reynolds shear stress arising from the compressibility effects on the mixing layers. From the previous results, it is clear that the proposed models' predictions are better than those obtained by their original models. Therefore, as a priority, the blending between different compressible models is seen as an important issue in the modeling of the pressure-strain correlation.

Author Contributions: Writing-original draft preparation, H.K.; writing-Review editing, H.K and A.B. All authors have read and agreed to the published version of the manuscript.

Funding: This research received no external funding.

Institutional Review Board Statement: Not applicable. **Informed consent Statement:** Not applicable.

Data Availability Statement: Not applicable.

Conflicts of Interest: The authors declare no conflict of interest.

Nomenclature

p	Pressure
T	Temperature
t	Time
a	Speed of sound
b_{ij}	Reynolds stress anisotropy
c_p	Specific heat at constant pressure
c_v	Specific heat at constant volume
R	Ideal gas constant
R_{ij}	Reynolds stress
M_t	Turbulent mach number
M_g	Gradient mach number
M_c	Convective mach number
K	Turbulent kinetic energy
u_i	Velocity in the direction x_i
d'	Fluctuation of the dilatation
$(\cdot)_{,i}$	x_i -derivative
Greek symbols	
γ	Specific heat ratio
ε	Turbulent dissipation
ε_s	Solenoidal dissipation
ε_c	Compressible dissipation
ρ	Density
μ	Viscosity coefficient
κ	Thermal conductivity coefficient
$\pi d = \overline{p' d'}$	Pressure–dilatation correlation
P_{ij}^*	Deviator of the pressure-strain tensor
δ_{ij}	Kronecker delta
τ_{ij}	Viscous stress tensor
Statistic symbols	
$(\cdot)''$	Favre fluctuation
$(\cdot)'$	Reynolds fluctuation
(\cdot)	Favre averaged
$\overline{(\cdot)}$	Reynolds averaged

References

- Blaisdell, G.A.; Mansour, N.N.; Reynolds, W.C. Compressibility effects on the growth and structure of homogeneous turbulent shear flow. *J. Fluid Mech.* **1983**, *256*, 443–485. [[CrossRef](#)]
- Sarkar, S.; Erlebacher, G.; Hussaini, M.Y.; Kress, H.O. The analysis and modeling of dilatational terms in compressible turbulence. *J. Fluid Mech.* **1991**, *227*, 473–493. [[CrossRef](#)]
- Sarkar, S. The stabilizing effects of compressibility in turbulent shear flows. *J. Fluid Mech.* **1995**, *282*, 163–186. [[CrossRef](#)]
- Simone, S.; Coleman, G.N.; Cambon, C. The effect of compressibility on turbulent shear flow: A rapid distortion-theory and direct numerical simulation study. *J. Fluid Mech.* **1997**, *330*, 307–338. [[CrossRef](#)]
- Fujihiro, H. Effects of pressure fluctuations on turbulence growth compressible homogeneous shear flow. *Phys. Fluid.* **1999**, *11*, 1623–1635.
- Vreman, A.W.; Sandham, N.D.; Luo, K.H. Compressible mixing layer growth rate and turbulence characteristics. *J. Fluid Mech.* **1996**, *330*, 235–258. [[CrossRef](#)]
- Goebel, S.G.; Dutton, J.C. Experimental study of compressible mixing layers. *AIAA J.* **1991**, *29*, 538–546. [[CrossRef](#)]
- Samimy, M.; Elliot, G.S. Effects of compressibility on the characteristics of the free shear layers. *AIAA J.* **1990**, *89*, 439–445. [[CrossRef](#)]
- Pantano, C.; Sarkar, S. A study of compressibility effects in the high speed turbulent shear layer direct simulation. *J. Fluid Mech.* **2002**, *451*, 329–371. [[CrossRef](#)]
- Foysi, H.; Sarkar, S. The compressible mixing layers: An LES study. *Theor. Comput. Fluid Dyn.* **2010**, *24*, 565–588. [[CrossRef](#)]
- Adumitroaie, V.; Ristorcelli, J.R.; Taulbee, D.B. Progress in Favre Reynolds stress closures for compressible flows. *Phys. Fluids* **1999**, *A11*, 2696–2719. [[CrossRef](#)]
- Hung, S.; Song, F. Modelling of pressure strain correlation compressible turbulent flow. *Acta Mech. Sin.* **2008**, *24*, 37–43. [[CrossRef](#)]

13. Hamed, M.; Hechmi, K.; Taieb, L. Extension of the Launder Reece and Rodi on Homogeneous shear flow. *Eur. Phys. J. B* **2005**, *45*, 147–154.
14. Launder, B.E.; Reece, G.J.; Rodi, W. Progress in the development of a Reynolds-stress turbulence closure. *J. Fluid Mech.* **1975**, *68*, 537–566. [[CrossRef](#)]
15. Hechmi, K.; Taieb, L. On the compressibility effects in mixing layers. *Therm. Sci.* **2016**, *20*, 1473–1484.
16. Speziale, C.G.; Sarkar, S. *Second Order Closure Models for Supersonic Turbulent Flows*; ICASE Report; NASA Langley Research Center: Hampton, VA, USA, 1991.
17. Zeman, O. Dilatational dissipation, the concept and application in modeling compressible mixing layers. *Phys. Fluids* **1990**, *A2*, 178–188. [[CrossRef](#)]
18. Blaisdell, G.A.; Sarkar, S. Investigation of the pressure-strain correlation in compressible homogeneous turbulent shear flow. *ASME-Publ.-FED* **1993**, *151*, 133–138.
19. Park, C.H.; Park, S.O. Compressible turbulence model for the pressure strain correlation. *J. Turbul.* **2005**, *6*, 1–24. [[CrossRef](#)]
20. Hechmi, K.; Taieb, L. A compressibility correction of the pressure strain correlation model in turbulent flow. *Comptes Rendus Mécanique* **2013**, *341*, 567–581.
21. Speziale, C.G.; Abid, R.; Mansour, N. Evaluation of Reynolds stress turbulence closures in compressible homogeneous shear flow. *J. Appl. Math. Phys.* **1995**, *46*, 5717–5736.
22. Freund, J.B.; Lele, S.K.; Monin, P. Compressibility effects in a turbulent annular mixing layer. *J. Fluid Mech.* **2000**, *421*, 229–267. [[CrossRef](#)]